Research Square

Preprints are preliminary reports that have not undergone peer review.
They should not be considered conclusive, used to inform clinical practice,
or referenced by the media as validated information.

RC-MIFT: Sharp Robustness Bounds and Screening-Conditioned Response in Materials

Idrees Oreibi

idrees114af@gmail.com

Directorate of Education Babylon, Ministry of Education, Iraq, Babil

Rehab Shather Abdul Hamza

Directorate of Education Babylon, Ministry of Education, Iraq, Babil

Research Article

Keywords: Material Response, Lattice Dynamics, Peierls Model, Robustness Bounds, Schur ComplementDensity Functional Perturbation Theory (DFPT)

Posted Date: September 17th, 2026

DOI: https://doi.org/10.21203/rs.3.rs-11061373/v1

License: This work is licensed under a Creative Commons Attribution 4.0 International License.
Read Full License

Additional Declarations: The authors declare no competing interests.

RC-MIFT: Sharp Robustness Bounds and Screening-Conditioned Response in Materials

Idrees Oreibi[1,*] and Rehab Shather Abdul Hamza[1,†]

[1] *Directorate of Education Babylon, Ministry of Education, Iraq, Babil*

Material response can be far more fragile than the underlying static energy because internal degrees of freedom relax and screen an externally probed coordinate. We formulate this effect as a task-aligned Schur-complement problem and derive sharp, nonasymptotic robustness bounds for simultaneous perturbations of hidden curvature, bare task stiffness, and coupling. The central screening leverage, $\kappa = \lambda_{\max}(S, D)$ with $S = C^T K^{-1} C$ and $D = A - S$, fixes both the surviving stiffness fraction $1/(1+\kappa)$ and the structured amplification of block errors. For equal normalized error budgets the exact task-Hessian distortion is $\mathcal{R}_{\rm eq}(\delta) = \delta(1 + 4\kappa - \delta)/(1 - \delta)$; a 5% frequency guarantee therefore forces the admissible block error to collapse as $\delta_{5\%} \sim 1/\kappa$ and, for screening-driven softening, as $\omega^2_{\rm soft}$. We prove a black-box energy theorem for projected response extraction, state finite-source and state-transfer no-go results, and audit the formulas numerically. Published data provide a 42-record stable response corpus, 72 mode-resolved matched cDFPT/DFPT cases, a near-critical meta-nitroaniline anchor with $\kappa = 48.108$, a same-source TaS_2 screening-driven stability crossing, and a 12-state Peierls-model sequence approaching $D \to 0^+$. The data support screening as a conditioning coordinate rather than a universal one-variable error law.

I. INTRODUCTION

First-principles calculations are routinely judged by energies, forces, relaxed structures, or selected observables. Such checks do not by themselves certify response. A material can match its reference energy at sampled configurations yet respond incorrectly to an infinitesimal field, strain, displacement, or collective coordinate because response depends on curvature and on how hidden degrees of freedom are allowed to relax. In density-functional perturbation theory (DFPT), constrained DFPT (cDFPT), electron-lattice downfolding, and elasticity, this hidden relaxation is often precisely the physical screening one wishes to describe [1–3, 5].

The question addressed here is therefore not whether screening exists, but how screening conditions the reliability of a calculated task response. We develop RC-MIFT (Response Conditioning and Screening in Materials) around three requirements. First, the conditioning coordinate must be invariant under natural rescalings and directly connected to the surviving stiffness. Second, robustness statements must be sharp for a declared perturbation model rather than heuristic. Third, the theory must remain auditable even when explicit second-derivative internals are unavailable.

The resulting structure is simple. Hidden relaxation subtracts a positive screening term from the bare task stiffness. The ratio of removed to surviving stiffness defines a generalized leverage κ. Large κ means that the observable is produced by cancellation of two much larger quantities, so errors in either block can be strongly amplified. The mathematics is a Schur complement, but the material consequence is a quantitative accuracy threshold that becomes singular at screening-driven softening.

* idrees114af@gmail.com

† alamerirehab300@gmail.com

II. SCREENING GEOMETRY AND SHARP ROBUSTNESS

Near a stable reference state, partition hidden coordinates x and task coordinates q and expand

$$E(x,q) = E_0 + \frac{1}{2}\begin{pmatrix} x \\ q \end{pmatrix}^T \begin{pmatrix} K & C \\ C^T & A \end{pmatrix} \begin{pmatrix} x \\ q \end{pmatrix} + O(3), \quad (1)$$

with $K > 0$. Minimizing over x gives $x_*(q) = -K^{-1}Cq$ and the relaxed task Hessian

$$\boxed{D = A - C^T K^{-1} C}, \qquad S \equiv C^T K^{-1} C = A - D \succeq 0. \quad (2)$$

Thus internal relaxation can only reduce task curvature within this positive quadratic setting. All generalized-eigenvalue and relative-norm statements below are restricted to the stable task subspace on which $D \succ 0$ (and hence $A \succ 0$); unstable and null directions are treated separately and are not assigned a positive-stiffness leverage.

Whitening the blocks by their bare metrics defines $G = K^{-1/2} C A^{-1/2}$. Then $A^{-1/2} S A^{-1/2} = G^T G$ and $A^{-1/2} D A^{-1/2} = I - G^T G$. Let

$$\phi = \lambda_{\max}(S, A) = \|G\|_2^2, \qquad \kappa = \lambda_{\max}(S, D). \quad (3)$$

The two are exactly related by

$$\boxed{\phi = \frac{\kappa}{1+\kappa}}, \qquad \boxed{1 - \phi = \frac{1}{1+\kappa}}. \quad (4)$$

The second identity gives the smallest fraction of bare stiffness that survives screening along the most conditioned task direction.

Now perturb all three blocks, $\widetilde{K} = K + \Delta K$, $\widetilde{A} = A + \Delta A$, and $\widetilde{C} = C + \Delta C$, and define whitened uncertainty

radii

$$\epsilon = \|K^{-1/2}\Delta K K^{-1/2}\|_2 < 1, \tag{5}$$

$$\alpha = \|A^{-1/2}\Delta A A^{-1/2}\|_2 < 1, \tag{6}$$

$$\zeta = \frac{\|K^{-1/2}\Delta C A^{-1/2}\|_2}{\|G\|_2}, \qquad \|G\|_2 > 0. \tag{7}$$

The relative coupling radius ζ is undefined when $G = 0$. In that case one uses the absolute radius $\xi = \|K^{-1/2}\Delta C A^{-1/2}\|_2$; the stability condition below becomes $\xi^2 < (1-\epsilon)(1-\alpha)$, and the corresponding worst-case relative distortion is $\alpha + \xi^2/(1-\epsilon)$. For these norm balls, uniform positivity of the perturbed relaxed Hessian is equivalent to the sharp condition

$$\boxed{\phi(1+\zeta)^2 < (1-\epsilon)(1-\alpha)}. \tag{8}$$

Aligned perturbations along the extremal singular directions saturate the boundary, establishing necessity as well as sufficiency for the declared uncertainty model.

Define the relative task-Hessian error by the stable-subspace spectral norm

$$R(\Delta K, \Delta A, \Delta C) = \left\| D^{-1/2}(\widetilde{D} - D)D^{-1/2} \right\|_2, \tag{9}$$

and let $\mathcal{R}_{\max}$ be its supremum over the three declared norm balls. The same extremal construction gives

$$\boxed{\mathcal{R}_{\max} = (1+\kappa)\alpha + \frac{\kappa(\epsilon + 2\zeta + \zeta^2)}{1-\epsilon}}. \tag{10}$$

For small block errors, $\mathcal{R}_{\max} \simeq (1+\kappa)\alpha + \kappa\epsilon + 2\kappa\zeta$: the coupling error enters twice at leading order because C appears on both sides of the screening quadratic form.

Setting $\epsilon = \alpha = \zeta = \delta$ yields

$$\boxed{\mathcal{R}_{\mathrm{eq}}(\delta) = \frac{\delta(1+4\kappa-\delta)}{1-\delta}}, \qquad \chi_{\mathrm{screened}} = 1 + 4\kappa. \tag{11}$$

If a relative frequency error no larger than τ is required, the corresponding stiffness distortion must satisfy $R \le \beta_\tau = 2\tau - \tau^2$. Solving $\mathcal{R}_{\mathrm{eq}}(\delta_\tau) = \beta_\tau$ gives

$$\delta_\tau = \frac{2\beta_\tau}{1 + 4\kappa + \beta_\tau + \sqrt{(1+4\kappa+\beta_\tau)^2 - 4\beta_\tau}}. \tag{12}$$

For $\kappa \gg 1$, $\delta_\tau \sim \beta_\tau/(4\kappa)$. If a clean screened mode obeys $A \propto \omega_{\mathrm{bare}}^2$ and $D \propto \omega_{\mathrm{soft}}^2$ with finite bare scale, then

$$\boxed{\delta_\tau \sim \frac{\beta_\tau}{4}\frac{\omega_{\mathrm{soft}}^2}{\omega_{\mathrm{bare}}^2}}. \tag{13}$$

Equation (13) is the conditional RC-MIFT critical robustness-collapse prediction; Eq. (12) is the exact algebraic result.

III. BLACK-BOX RESPONSE AUDITING AND NO-GO RESULTS

The theory is useful only if it can be tested without privileged access to a code's internal Hessian. Introduce a source matrix F through $E_\lambda(x) = E(x) + \langle F\lambda, x\rangle$. Let $x_*(\lambda)$ be the smooth local stationary branch continuing a stable nondegenerate reference minimum, and define $G(\lambda) = E_\lambda(x_*(\lambda))$. Then

$$\boxed{-\nabla_\lambda^2 G(0) = F^T K^{-1} F}. \tag{14}$$

Projected susceptibility can therefore be extracted from ordinary self-consistent total energies. A central difference is second order, while Richardson combination raises the leading order to four. The numerical audit recovers orders 2.00036 and 4.00002, respectively.

Two limitations are equally important. First, a finite set of sources certifies only the probed span. The extremal relative distortions on that span are generalized eigenvalues of $(S_\theta - S_*)v = \delta S_* v$, but finitely many passing probes do not establish a global curvature certificate unless completeness or saturation is separately justified. Second, agreement at a common configuration does not automatically transfer to each model's independently relaxed equilibrium. A conditional transfer bound requires strong convexity, Hessian Lipschitz control, and a residual force or pressure. These no-go statements prevent static agreement from being promoted to an unearned global response claim.

The formal implementation was stress-tested on 20,000 random three-block problems: no violation of Eq. (10) was observed and the maximum sampled ratio of actual distortion to the bound was 1.000000000000004. Independent solver and frequency-propagation audits likewise showed zero bound violations in their declared domains. These computations audit the implementation and sharpness construction; they are not substitutes for the proof.

IV. PUBLISHED-DATA EVIDENCE

We next asked whether published materials occupy the conditioning regimes implied by the theory. A direct-response corpus assembled from clamped/relaxed elastic and response data contains 46 observations from ten independent sources; 42 satisfy the positive-A, positive-D, positive-semidefinite-S gates and four are retained as red-team cases. Across valid records,

$$0.002664 \le \kappa \le 48.108. \tag{15}$$

The upper tail is not a numerical artifact of averaging: full tensors are retained whenever available and generalized eigenvalues are computed in the published units.

A stricter matched analysis uses cDFPT/DFPT mode pairs with state and mode identity controlled within the

source protocol. It yields 72 Level-A mode-resolved observations in benzene, graphene, and CsV_3Sb_5, plus a Level-C ZnO tensor/experiment cross-check [1, 2, 9]. Within the two released approximation protocols, source-controlled ranks show a positive pooled tendency ($\rho = 0.780$; one-sided stratified permutation $p \simeq 5.0 \times 10^{-5}$), but the 2.5–97.5 material-cluster resampling percentile range is broad, $[-0.141, 0.987]$. With only three material clusters, this range is a stability diagnostic rather than a calibrated confidence interval. Figure 1 therefore reports the source-separated data rather than a universal pooled fit. Pointwise counterexamples exist, and RC-MIFT does not posit a deterministic law $e = f(\kappa)$.

A. Breadth, reconstruction, and red-team retention

The direct-response corpus was deliberately assembled from heterogeneous published settings rather than a single convenient family. It includes three-dimensional and two-dimensional elastic datasets, multiple functionals, molecular and inorganic crystals, and a raw-response reconstruction test from ABINIT tutorial data. For the latter, the archived K, C, and rigid-ion A blocks reconstruct the independently printed relaxed tensor through $D = A - C^T K^+ C/V$ with a maximum absolute residual of 6.73×10^{-6} GPa after projecting the translational null space. Because the tutorial uses a deliberately modest cutoff, this record is treated as a methodological closure test, not as production materials evidence.

The audit also retains failures. One $BaTiO_3$ Hartree–Fock record has nonpositive relaxed stiffness; three other published pairs yield a slightly indefinite $S = A - D$ at printed precision and remain quarantined rather than repaired post hoc. Likewise, an early apparent TaS_2 value $\kappa \sim 829$ was traced to acoustic residuals at Γ and removed by explicit translational projection, while an apparent 98.45% `qe2screen` spectral error was traced to a source-unit mismatch. Both corrections remain documented in the archive. This policy matters because near criticality small denominators make exactly these failure modes look artificially compelling.

V. NEAR-CRITICAL STABLE ANCHOR AND STABILITY CROSSING

Meta-nitroaniline (mNA) supplies a particularly transparent stable-side anchor. The elastic table of Wang *et al.* reports, for the same C_{66} shear direction, a clamped-ion value $A = 157.735$ GPa, a relaxed-ion value $D = 3.212$ GPa, and an external comparison value 4.26 GPa [7]. That table attributes the comparison entry to Avanci *et al.*, whose experiment used synchrotron x-ray multiple diffraction [8]; it is not the ultrasonic value of Bain *et al.* Hence

$$\kappa = \frac{A - D}{D} = 48.108, \qquad \phi = 0.979637, \qquad (16)$$

so only 2.036% of the clamped stiffness survives while D remains positive. The relaxed-DFPT difference relative to the externally listed comparison value is 24.60%. For a 5% frequency target, Eq. (12) gives an equal-budget radius $\delta_{5\%} = 5.04 \times 10^{-4}$. This is a near-critical stable anchor, not a claim that the tabulated comparison is a same-condition test or that its discrepancy equals the theorem's worst-case bound.

Published 1H-TaS_2 data provide the complementary side of the boundary [5, 6]. For a 3×3 CDW distortion, the paired cDFPT and DFPT interatomic-force-constant matrices yield a partially screened curvature $A_{\mathrm{partial}} = +0.679136$ eV/α^2 and a fully screened curvature $D_{\mathrm{full}} = -0.087241$ eV/α^2. Therefore

$$S_{\mathrm{active}} = 0.766377 \text{ eV}/\alpha^2, \qquad \phi_{\mathrm{active}} = 1.12846 > 1. \qquad (17)$$

The positive-D theorem no longer applies; instead, the result is direct same-source evidence that the added active-subspace screening crosses the stability boundary. A local curvature fitted independently from the published DFT energy curve differs from the IFC curvature by only 3.7% in the smallest retained amplitude window. Figure 3 places mNA and TaS_2 on opposite sides of $\phi = 1$.

VI. A STABLE PATH TO THE CRITICAL BOUNDARY

The public `qe2screen` model distributed with Berges *et al.* provides a controlled sequence in which the same scalar Peierls phonon at fixed $q = 2k_F = 2\pi/3$ is followed through 12 stable electronic temperatures [3, 4]. The screened stiffness decreases from 2.071×10^{-3} to 1.962×10^{-6} eV^2, while κ grows from 0.811 to 1910.7. For the mixed bare-screened-vertex approximation Π^{b0}, the independently evaluated spectral-peak error relative to direct RPA increases from 0.17% to 41.8%, with Spearman $\rho = 1$ and Kendall $\tau = 1$. Removing the closest-to-critical point leaves $\rho = 1$.

The same sequence also supplies a built-in falsification control. The two-screened-vertex approximation Π^{00} remains below 0.82%, saturates in the four closest states, and decreases slightly at the most critical point. Thus even extreme κ does not dictate a unique error magnitude or exponent. Figure 4 shows this contrast. A Theil–Sen fit of the mixed-vertex relation $e \propto (\omega^2_{\mathrm{soft}})^p$ gives $p = -0.710832$; 10,000 seeded row-resampling replicates give a 2.5–97.5% percentile range $[-1.242430, -0.513667]$. This range is a finite-sample stability diagnostic, and the model-internal scaling is not an empirical verification of Eq. (13) for the admissible uncertainty radius.

VII. NUMERICAL PRECISION NEAR SCREENED SOFTENING

The physical conditioning quantified by κ is only one source of fragility. The numerical extraction of a small

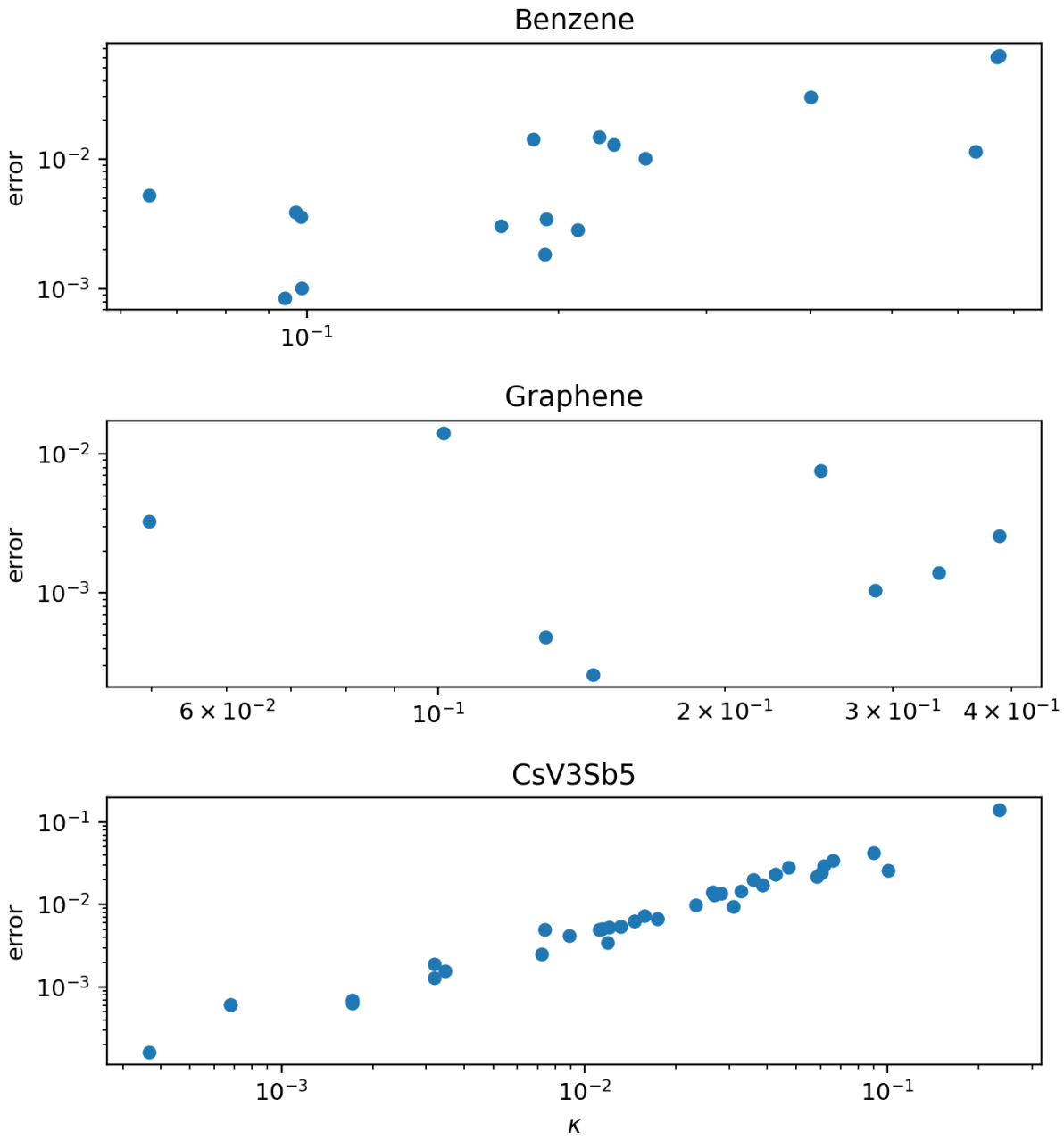


FIG. 1. Stable matched mode-resolved cases extracted from published cDFPT/DFPT data. Error definitions are source-specific and are not pooled in raw units. CsV_3Sb_5 exhibits a strong within-protocol ordering, whereas benzene and graphene show weaker and nonmonotone behavior. This protocol dependence is consistent with Eq. (10), in which κ sets amplification capacity but realized error also depends on the block-error structure.

curvature from finite-energy or finite-force data becomes separately ill conditioned as the mode softens. For a pth-order energy-based second derivative, write the total curvature error schematically as

$$E_{\mathrm{curv}}(h) \lesssim ah^p + b\frac{\tau_E}{h^2}, \tag{18}$$

where the first term is truncation error and τ_E is the energy noise floor. Provided this two-term asymptotic error model is valid over the optimizing step range and the prefactors a and b are finite and nonzero, optimizing the step gives $E_{\mathrm{min}} \propto \tau_E^{p/(p+2)}$. If, in addition, $D = c\omega^2$ with finite nonzero c and one demands an absolute curvature error proportional to D, then

$$\boxed{\tau_E = O(\omega^{2+4/p})}. \tag{19}$$

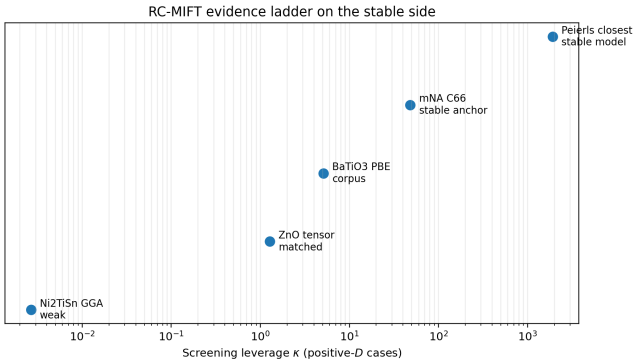


FIG. 2. Stable-side evidence spans more than five decades in screening leverage, from weakly screened elastic records to the mNA near-critical material anchor and the closest stable point of the published Peierls model. The plotted points have different evidential roles and are not treated as one regression dataset.

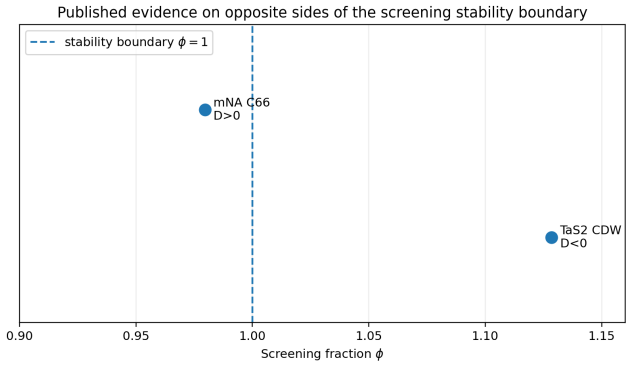


FIG. 3. Published evidence on opposite sides of the screening stability boundary. mNA remains stable with $\phi = 0.979637$, whereas the TaS_2 CDW direction has $\phi_{\text{active}} = 1.12846$ and $D < 0$.

Thus a standard second-order energy curvature requires $\tau_E = O(\omega^4)$, while a fourth-order construction requires $O(\omega^3)$. For force differences, under the analogous valid two-term model with finite nonzero prefactors, the noise term scales as τ_F/h and the corresponding requirement is

$$\boxed{\tau_F = O(\omega^{2+2/p})}, \tag{20}$$

so a second-order force difference requires $\tau_F = O(\omega^3)$. The archived theory suite verifies the predicted exponents to numerical precision. These relations are distinct from Eq. (13): Eq. (13) is a physical block-error tolerance induced by screening, whereas Eqs. (19) and (20) specify how the numerical noise floor must tighten merely to resolve the shrinking stiffness. Near a soft-mode boundary the two constraints act simultaneously.

This distinction also motivates the black-box protocol of Eq. (14). Richardson cancellation improves the truncation order without changing the underlying self-consistent method, and a measured convergence order provides a falsifier for the assumed finite-difference regime. Likewise, the archived solver-residual certificate bounds the response error of an inexact hidden-variable solve in its natural energy metric rather than demanding an arbitrary absolute residual. Together these checks separate physical conditioning, discretization error, and iterative-solver error instead of folding them into a single unexplained discrepancy.

VIII. SCOPE, FALSIFIERS, AND IMPLICATIONS

The evidence establishes three distinct statements and leaves two important tests open. First, the three-block robustness condition and $\mathcal{R}_{\max}$ are exact and sharp for the declared norm-bounded perturbation model. Second, published materials span weak to near-critical screening leverage, and same-source TaS_2 data show a screening-driven crossing of the stability boundary. Third, matched cDFPT/DFPT and model data show that realized errors can grow strongly with screening within fixed protocols, but can also remain small when the block-error structure is favorable.

What is *not* established is equally explicit. The archive does not contain a real-material multi-point near-critical sequence with an independent error at every state, and it does not reconstruct ϵ, α, and ζ independently in a real material, so a direct material test of Eq. (10) remains open. These are falsifiable next-step targets rather than hidden assumptions.

A practical consequence follows already. Near screening-driven softening, the accuracy budget required of the underlying blocks can become far tighter than static-energy benchmarks suggest. Moreover, numerical differentiation itself becomes more demanding: for a pth-order energy-based second derivative, keeping absolute curvature error proportional to $D \propto \omega^2$ requires energy noise $\tau_E = O(\omega^{2+4/p})$; for a pth-order force difference, $\tau_F = O(\omega^{2+2/p})$. Response certification near soft modes therefore requires both a physically conditioned error budget and a commensurate numerical precision budget.

IX. CONCLUSION

RC-MIFT turns relaxation-induced screening into a quantitative robustness coordinate. The same generalized eigenvalue κ that measures removed versus surviving stiffness controls a sharp structured error amplification, yields an exact stability radius, and predicts a quadratic collapse of admissible block error under screening-driven softening. The framework is auditable from black-box energies, includes explicit no-go rules against overclaiming finite-source or state-transfer success, and is supported by published data spanning weak screening, a near-critical stable material anchor, a model sequence approaching

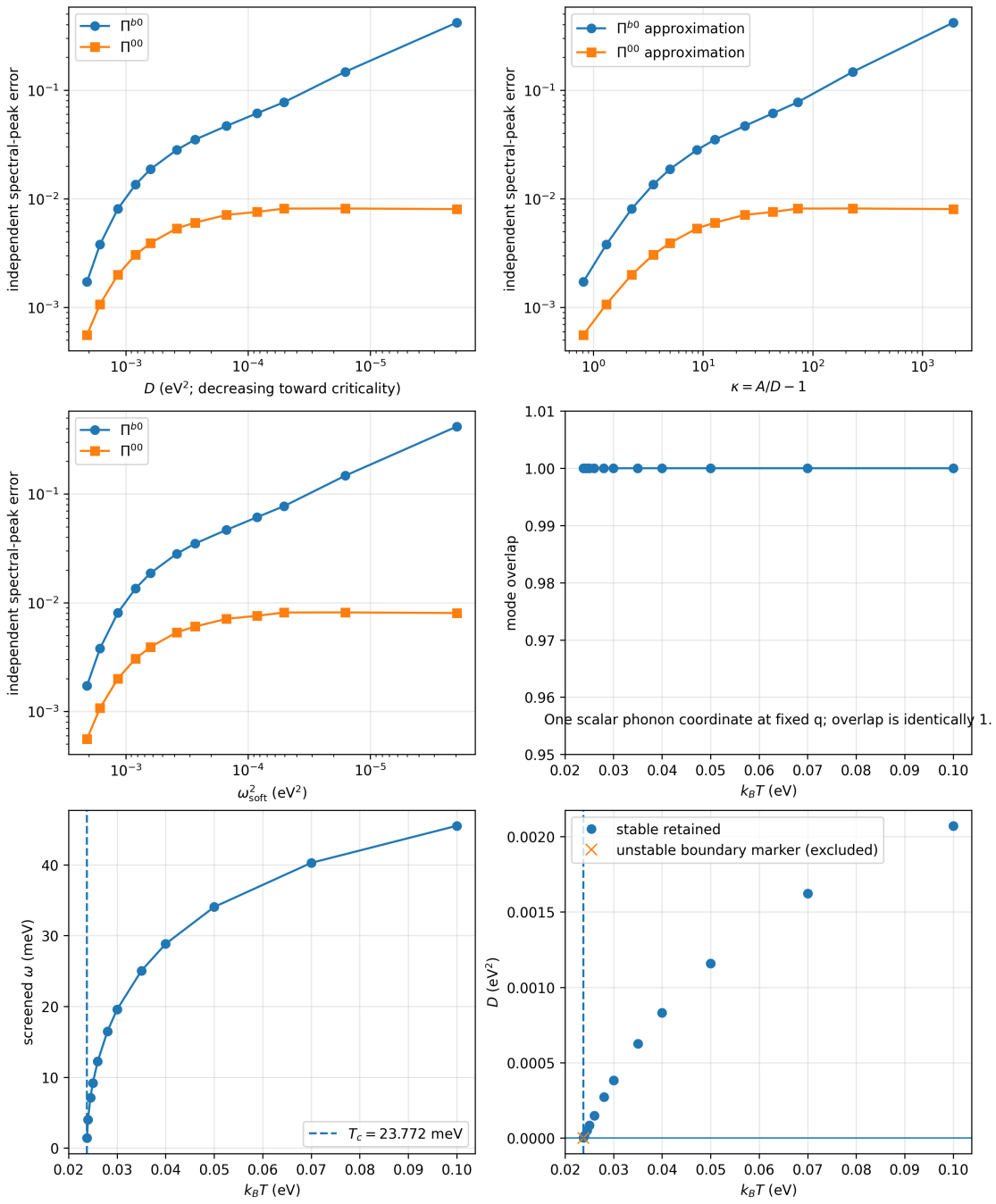


FIG. 4. Published Peierls-model sequence approaching the stable critical boundary. The mixed-vertex approximation (blue in the source figure) develops a large error as $D \to 0^+$ and κ grows, whereas the two-screened-vertex control saturates below 1%. The bottom row marks the screened softening and the first unstable audit point, which is excluded from stable fits.

$D \to 0^+$, and a real-material screening-driven instability crossing. The central lesson is not that screening uniquely determines error, but that screening determines how unforgiving a response problem can become.

ACKNOWLEDGMENTS

OpenAI ChatGPT (GPT-5.6 Sol) and the Codex Work interface were used substantively during September 2026 for proof exploration, literature checking, Python implementation, numerical stress tests, figure preparation, data-audit assistance, and manuscript preparation. The authors specified the research questions, assumptions,

TABLE I. Evidence hierarchy and present claim status. "Sharp" refers to the declared norm-bounded perturbation model, not to an empirical universal error law.

Result	Status	Evidence and boundary
Three-block stability and $\mathcal{R}_{\max}$	proved sharp	Exact derivation; aligned perturbations saturate the boundary; 20,000 random audits with zero violations.
Black-box projected response	proved exact	$-\nabla^2_\lambda G(0) = F^T K^{-1} F$ at a stable nondegenerate minimum; finite-source success is explicitly not promoted to a global certificate.
Published stable screening range	supported	42 valid direct-response records from 10 sources; $\kappa = 0.002664$–48.108 after red-team exclusions.
Near-critical stable material anchor	supported, Level C	mNA C_{66} has $\kappa = 48.108$ and $D > 0$; the 4.26 GPa comparison value is reproduced by Wang *et al.* and attributed there to the synchrotron-x-ray study of Avanci *et al.*, not to an ultrasonic benchmark.
Screening-driven instability crossing	supported boundary evidence	Same-source TaS_2 CDW IFCs give $\phi_{\text{active}} = 1.12846$ and $D < 0$; excluded from positive-D κ statistics.
Universal $e = f(\kappa)$ or real-material ω^2 law	not supported / open	Protocol dependence and pointwise counterexamples remain; no qualifying open real-material multi-point near-critical sequence was found.

and acceptance criteria and verified outputs using explicit derivations, generalized-eigenvalue checks, deterministic regression tests, bounded-perturbation tests, independent-data cross-checks, and reproducible simulations. The authors take full responsibility for the content.

DATA AND SOFTWARE AVAILABILITY

The accompanying reproducibility package contains the author-generated code and derived numerical tables selected for the reported results. Third-party raw files are not redistributed; canonical sources, filenames, versions, and available checksums are recorded in the external-data manifest. The published source records used here include Materials Cloud [4] and Zenodo [6]; additional source identifiers are listed in the Supplemental Material.

[1] X. Wu, D. Vanderbilt, and D. R. Hamann, "Systematic treatment of displacements, strains, and electric fields in density-functional perturbation theory," Phys. Rev. B **72**, 035105 (2005), doi:10.1103/PhysRevB.72.035105.

[2] E. G. C. P. van Loon, J. Berges, and T. O. Wehling, "Downfolding approaches to electron-ion coupling: Constrained density-functional perturbation theory for molecules," Phys. Rev. B **103**, 205103 (2021), doi:10.1103/PhysRevB.103.205103.

[3] J. Berges *et al.*, "Phonon Self-Energy Corrections: To Screen, or Not to Screen," Phys. Rev. X **13**, 041009 (2023), doi:10.1103/PhysRevX.13.041009.

[4] J. Berges *et al.*, `qe2screen` public data and code, Materials Cloud, doi:10.24435/materialscloud:he-pv.

[5] A. Schobert *et al.*, "Ab initio electron-lattice downfolding: Potential energy landscapes, anharmonicity, and molecular dynamics in charge density wave materials," SciPost Phys. **16**, 046 (2024), doi:10.21468/SciPostPhys.16.2.046.

[6] A. Schobert *et al.*, data for *Ab initio electron-lattice downfolding*, Zenodo (2024), doi:10.5281/zenodo.10514203.

[7] F. Wang *et al.*, "First-principles analysis of a molecular piezoelectric meta-nitroaniline," RSC Adv. **8**, 16991–16996 (2018), doi:10.1039/C8RA01499J.

[8] L. H. Avanci, L. P. Cardoso, S. E. Girdwood, D. Pugh, J. N. Sherwood, and K. J. Roberts, "Piezoelectric coefficients of mNA organic nonlinear optical material using synchrotron x-ray multiple diffraction," Phys. Rev. Lett. **81**, 5426–5429 (1998), doi:10.1103/PhysRevLett.81.5426.

[9] S. Enzner *et al.*, "Phonon fluctuation diagnostics: Origin of charge order in AV_3Sb_5 kagome metals," Phys. Rev. B (2026), doi:10.1103/czn6-ndzm.

[10] A. Mahmoud *et al.*, "Low-temperature phase of $BaTiO_3$: Piezoelectric, dielectric, elastic, and photoelastic properties from ab initio simulations," Phys. Rev. B **89**, 045103 (2014), doi:10.1103/PhysRevB.89.045103.